Synthesis, characterization, and optoelectronic properties of heteroleptic iridium complexes containing substituted 1,3,4-oxadiazole and β-diketone as ligands

Amit Kumar [a b] , Ritu Srivastava [a] , Partap S. Kadyan [b] , Modeeparampil N. Kamalasanan [a] & Ishwar Singh [b]

[a] Center for Organic Electronics (OLED Lab.) , National Physical Laboratory (Council of Scientific and Industrial Research) , Dr. K.S. Krishnan Road, New Delhi-110012 , India

[b] Department of Chemistry , Maharshi Dayanand University , Rohtak , Haryana-124001 , India
Published online: 31 Jan 2012.

PLEASE SCROLL DOWN FOR ARTICLE

Taylor & Francis
Taylor & Francis Group

Synthesis, characterization, and optoelectronic properties of heteroleptic iridium complexes containing substituted 1,3,4-oxadiazole and *β*-diketone as ligands

AMIT KUMAR†‡, RITU SRIVASTAVA*†, PARTAP S. KADYAN‡,
MODEEPARAMPIL N. KAMALASANAN† and ISHWAR SINGH‡

†Center for Organic Electronics (OLED Lab.), National Physical Laboratory
(Council of Scientific and Industrial Research),
Dr. K.S. Krishnan Road, New Delhi-110012, India
‡Department of Chemistry, Maharshi Dayanand University,
Rohtak, Haryana-124001, India

The new heteroleptic iridium(III) complexes (BuOXD)$_2$Ir(tta) and (BuOXD)$_2$Ir(tmd) [BuOXD = 2-(4-butyloxyphenyl)-5-phenyl[1,3,4]oxadiazolato-N4,C2, tta = 1,1,1-trifluoro-4-thienylbutane-2,4-dionato, tmd = 2,2,6,6-tetramethylheptane-3,5-dionato] have been synthesized and characterized. These complexes have two cyclometalated ligands (C^N) and a bidentate diketone ligand (X) [C^N)$_2$Ir(X)], where X is a *β*-diketone with trifluoromethyl, theonyl or *t*-butyl groups. The color tuning with the change in electronegativity of substituents in the *β*-diketones has been studied. Photoluminescence spectra of the complexes showed peak emissions at 523 and 549 nm, respectively. The electroluminescent properties of these complexes have been studied by fabricating multi layer devices with device structure ITO/*α*-NPD/8% iridium complex doped CBP/BCP/Alq$_3$/LiF/Al. The electroluminescence spectra also showed peak emissions at 526 and 570 nm for (BuOXD)$_2$Ir(tta) and (BuOXD)$_2$Ir(tmd), respectively. These metal complexes showed good thermal stability in air to 340°C.

Keywords: Heteroleptic iridium complex; *β*-Diketones; Electroluminescence; Color tuning

1. Introduction

Cyclometalated or oligopyridyl complexes of group 10 metals have unique photophysical properties [1–4] and focus on iridium(III) complexes has been given for fabricating organic light emitting devices (OLEDs) because of their good quantum yield, thermal stability, and high electroluminescence (EL) efficiency [5–11]. 1,3,4-Oxadiazole derivatives such as 2-(4-tert-butylphenyl)-5-(4-biphenyl)-[1,3,4]-oxadiazole (PBD) are widely used as electron-injecting/hole-blocking and excellent electron-transport material in multilayer OLEDs [12–16]. High electron affinity makes them good candidates for electron injection and transportation [17–19]. Recently some fluorinated 1,3,4-oxadiazole based heteroleptic iridium(III) complexes were reported

---

*Corresponding author. Email: ritu@mail.nplindia.ernet.in

where the emission was tuned to blue by dithiolate ancillary ligands [20]. There are also reports of mixed ligand complexes of iridium(III) using different β-diketones and 1,3,4-oxadiazoles for tuning the emission color [21]. Lamansky *et al.* [22] have shown that if triplet-state energy of the β-diketone (X) is lower than the $C^{\wedge}N^3(\pi-\pi^*)$ or ^{3}MLCT levels, the triplet X level will be the lowest energy excited state and a switch of emission from "$C^{\wedge}N_2$Ir" to X will be seen in a series of complexes prepared with different β-diketones (i.e., acetylacetone, 1,1,5,5-tetramethylacetylacetone, benzoylace-tonate, etc.) and its influence on color tuning of iridium complexes. In this way color is tuned in mixed ligand iridium complexes using different β-diketones with the same oxadiazole.

We report the synthesis and characterization of the new heteroleptic iridium(III) complexes (BuOXD)$_2$Ir(tta) and (BuOXD)$_2$Ir(tmd) [BuOXD = 2-(4-butyloxyphenyl)-5-phenyl[1,3,4]oxadiazolato-N4,C2, tta = 1,1,1-trifluoro-4-thienylbutane-2,4-dionato, tmd = 2,2,6,6-tetramethylheptane-3,5-dionato]. These complexes have two cyclometalated ligands (C$^{\wedge}$N) and one bidentate diketone ligand (X) represented as [(C$^{\wedge}$N)$_2$Ir(X)], where X is chosen to be different β-diketones with trifluoromethyl, thionyl, or *t*-butyl groups. Substitutions on the β-diketone lead to the alteration of electronic properties of the complexes as well as their emission color.

2. Experimental

2.1. *Materials*

The various chemicals used to synthesize ligand and metal complexes were purchased from Fluka. Solvents were used as supplied.

2.2. *Synthesis*

2.2.1. Synthesis of 1,3,4-oxadiazole ligand. The alkyl-oxy substituted oxadiazole was synthesized in a stepwise manner starting from *p*-hydroxymethylbenzoate as shown in scheme 1 of figure 1. *p*-Hydroxymethylbenzoate (32 mmol), bromobutane (40 mmol), and K$_2$CO$_3$ (72 mmol) were added to 100 mL dry DMF. The reaction mixture was refluxed at 80–90°C. Progress of the reaction was monitored by thin layer chromatography. After completion of reaction, the compound was extracted in chloroform. The solid product obtained after removal of solvent was further purified by column chromatography using 5% ethyl acetate in hexane as eluent giving pure *p*-butyloxymethylbenzoate.

p-Butyloxymethylbenzoate (24 mmol) and hydrazine hydrate (200 mmol) were taken in 50 mL methanol and refluxed overnight. Solid *p*-butyloxybenzylhydrazine obtained after the evaporation of excess methanol was washed several times with water. Further *p*-butyloxybenzylhydrazine (29 mmol), benzoyl chloride (35 mmol), LiCl (35 mmol), and triethylamine (43 mmol) were refluxed at 80°C in dry DMF producing 1-(*p*-butyloxybenzylcarbonyl)-2-benzylcarbonylhydrazine (BuAXD) which was finally refluxed in POCl$_3$ overnight to give 2-(4-butyloxyphenyl)-5-phenyl[1,3,4]oxadiazole (BuOXD). After every step products were purified by column chromatography (scheme 1 of figure 1).
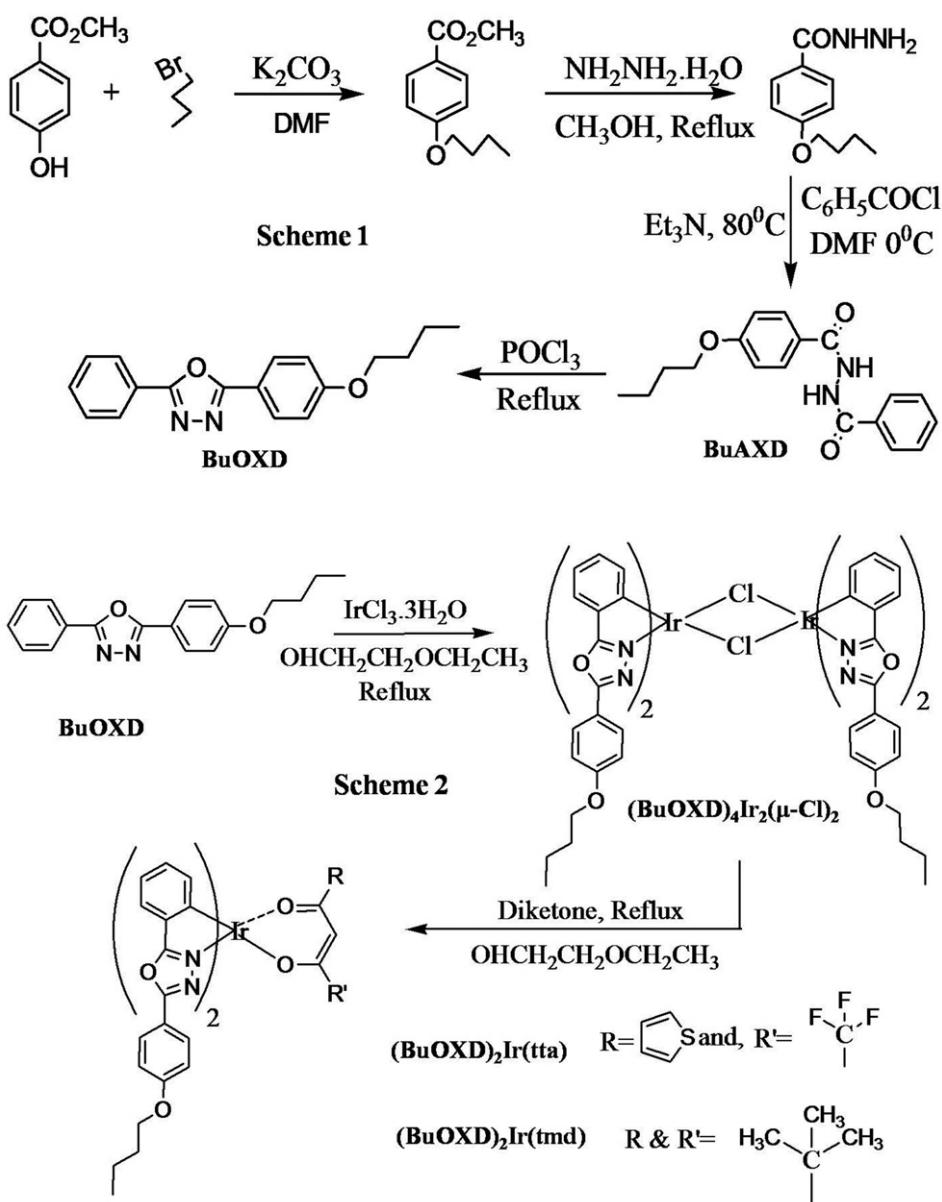
Figure 1.   Scheme 1: Synthetic route of BuOXD; Scheme 2: Synthetic route of binuclear and mononuclear iridium complexes.

(BuAXD) Yield 78%, FT-IR (neat) ν_{max}: 3194, 1578 (N–H); 2956 (C–H); 1626 (C=O from amide); 1126 (C–O–C); 840, 804, 741. Anal. Calcd for $C_{18}H_{20}N_2O_3$ (%): C, 69.23; H, 6.41; N, 8.97. Found (%): C, 69.12; H, 6.28; N, 8.68.

(BuOXD) Yield 82%, FT-IR (neat) ν_{max}: 2954(C–H); 1608 (C=N); 1582, 1551 (C=C); 1308, 1254 (C–O); 1121, 1068 (C–O–C); 686, 736. Anal. Calcd for $C_{18}H_{18}N_2O_2$ (%): C, 73.47; H, 6.12; N, 9.52. Found (%): C, 73.24; H, 5.97; N, 9.35.

2.2.2. Synthesis of binuclear iridium-oxadiazole complex. Tetrakis{2-(4-butyloxyphe-nyl)-5-phenyl[1,3,4]oxadiazolato-N4, C2}di(μ-chloro) diiridium(III) [(BuOXD)$_4$Ir$_2$ (μ-Cl)$_2$]. Iridium trichloride hydrate (0.5 mmol) and BuOXD (1.25 mmol) were added to 40 mL mixture of 2-ethoxyethanol and water (v/v = 3 : 1). The mixture was refluxed for 24 h and cooled to room temperature. The resulting solid was collected by filtration, washed with ethanol, water, and hexane, and pumped dry to give the crude chloro-bridged dimer.

(BuOXD)$_4$Ir$_2$(μ-Cl)$_2$ Yield 56%, FT-IR (neat) ν_{max}: 2954(C–H); 1608 (C=N); 1582, 1551 (C=C); 1308, 1254 (C–O); 686, 736.

2.2.3. Synthesis of mononuclear iridium-oxadiazole complexes. (BuOXD)$_2$Ir(tta) and (BuOXD)$_2$Ir(tmd). Without further purification, the dimer was added to a mixture of Na$_2$CO$_3$, diketone (tta or tmd) in 2-ethoxyethanol (30 mL). After reflux for 24 h, the reaction mixture was poured into water. The light brown precipitate was filtered off and washed with water, hexane, and ether (scheme 2 of figure 1).

(BuOXD)$_2$Ir(tta). Yield 82%, Photoluminescence (in ethanol) = 523 nm, FT-IR (neat) ν_{max}: 2954(C–H); 1608 (C=N); 1583, 1552 (C=C); 1300, 1253 (C–O); 1126, 1040 (C–O–C); 687, 737. Anal. Calcd for C$_{44}$H$_{39}$N$_4$O$_6$SF$_3$Ir (%): C, 52.8; H, 3.9; N, 5.6. Found (%): C, 52.42; H, 3.48; N, 5.29.

(BuOXD)$_2$Ir(tmd). Yield 84%, Photoluminescence (in ethanol) = 550 nm, FT-IR (neat) ν_{max}: 2953(C–H); 1609 (C=N); 1583, 1551 (C=C); 1301, 1253 (C–O); 1126, 1070 (C–O–C); 686, 736. Anal. Calcd for C$_{47}$H$_{54}$N$_4$O$_6$Ir (%): C, 58.63; H, 5.61; N, 5.82. Found (%): C, 58.47; H, 5.36; N, 5.35.

2.3. Instrumentation

C, H, and N analyses of the complexes were done by an Elemental Analyzer Perkin-Elmer 2400 CHN. Perkin-Elmer 2000 FTIR was used to record infrared (IR) spectra in KBr pellets. The UV-Vis spectra of complexes were recorded in CH$_2$Cl$_2$ solution using a UV-Vis spectrophotometer (Shimadzu 2401 PC). Photoluminescence (PL) spectra of the complexes were studied using a spectrofluorometer (Fluorolog Jobin Yvon-Horiba, model-3-11) at room temperature. The EL spectrum was recorded with a high resolution spectrometer (Ocean Optics HR-2000CG UV-NIR). The current–voltage–luminescence (I–V–L) characteristics was measured with a luminance meter (LMT l-1009) interfaced with a Keithley 2400 programmable voltage–current digital source meter. All the measurements were performed at room temperature and under ambient atmosphere, without any encapsulation.

2.4. OLED device fabrication and characterizations

Indium-tin oxide (ITO) coated glass substrate with a sheet resistance $20 \, \Omega \, cm^{-2}$ was used as anode which was patterned and cleaned using deionized water, acetone, trichloroethylene, and isopropyl alcohol sequentially for 20 min using an ultrasonic bath and dried in a vacuum oven. The hole transporting layer and the emitting layers were deposited on the substrate sequentially under high vacuum (1×10^{-5} torr) at a deposition rate of $0.1 \, Ås^{-1}$. The thickness of the deposited film was monitored *in-situ* by

quartz crystal. 300 Å of *N,N*-diphenyl-*N,N*-bis(1-naphthyl)-1,1-biphenyl-4,4-diamine (α-NPD) as the hole transporting layer; 350 Å of the (8%) complex (BuOXD)$_2$Ir(tta) or (BuOXD)$_2$Ir(tmd) doped in 4,4'-biscarbazolylbiphenyl (CBP) as the emitting layer; 60 Å of 2,9-dimethyl 4,7-diphenyl-1,10-phenanthroline (BCP) as a hole and exciton blocking layer (HBL), 280 Å of tris(8-hydroxyquinolinato)aluminum (Alq$_3$) as electron transport layer, and a cathode comprising 10 Å lithium fluoride and 1000 Å aluminum were sequentially deposited onto the substrate to complete the device structure.

3. Results and discussion

3.1. *Material synthesis and characterization*

We synthesized new iridium complexes bearing 1,3,4-oxadiazole and β-diketone based ligands with procedures previously reported by Dedeian *et al.* [23–25]. The syntheses of the ligands and iridium complexes are depicted in schemes 1 and 2 of figure 1. The synthetic method used to prepare these complexes involved two steps. In the first step, IrCl$_3 \cdot$3H$_2$O was allowed to react with an excess of the cyclometalated ligand (2.5 times) to give a chloro-bridged dinuclear complex, i.e. (BuOXD)$_4$Ir$_2$(μ-Cl)$_2$. The chloro-bridged dinuclear complex could readily be converted to mononuclear complexes (BuOXD)$_2$Ir(X) by replacing the two bridging chlorides with a bidentate β-diketone, finally producing iridium(III) octahedrally coordinated by three chelating ligands. The coordination geometry of the "(BuOXD)$_2$Ir" fragment in the mononuclear complex is the same as that for the dinuclear complexes. Thermal studies showed that all the mononuclear iridium complexes with different β-diketones were thermally stable to 340°C. As indicated by the NMR data, the maximum high-field chemical shift is observed for the proton to the ortho-metalated carbon that experiences the largest shielding of any of the ligand protons. The (BuOXD)$_2$Ir(X) complexes are stable in air and could be sublimed in vacuum without decomposition before device fabrication.

3.2. *UV-Vis absorption and PL spectra*

UV-Vis absorption and PL spectra for the oxadiazole ligand and iridium metal complexes were measured in CH$_2$Cl$_2$. The relevant spectral characteristics are given in figure 2. Oxadiazole derivatives exhibited strong absorption bands at 250–350 nm from π–π* electronic transitions focusing on the conjugated oxadiazole moieties [26].

As shown in curve A of figure 2(a), the peak at 296 nm is due to UV-absorption of the π–π* electronic transitions of oxadiazole ligand. Curves B and C in figure 2(a) show absorption spectra of free tta and (BuOXD)$_2$Ir(tta) complex, respectively. Figure 2(a) curves D and E show absorption spectra of the free tmd and (BuOXD)$_2$Ir(tmd), respectively. By comparing absorption spectra of free ligands, the intense absorptions in the ultraviolet region of the spectra, between 250 and 350 nm, can be assigned to ligand-centered, spin-allowed ^{1}π–π* electronic transitions. Relatively weaker absorptions at 350–400 nm are well-resolved, ascribed to a spin-allowed, metal-to-ligand charge transfer (^{1}MLCT) transition. The long tail extended to lower energies (400–500 nm), likely associated with both ^{3}MLCT and ^{3}π–π* transitions, which gain considerable intensity by mixing with the ^{1}MLCT transition through spin–orbit
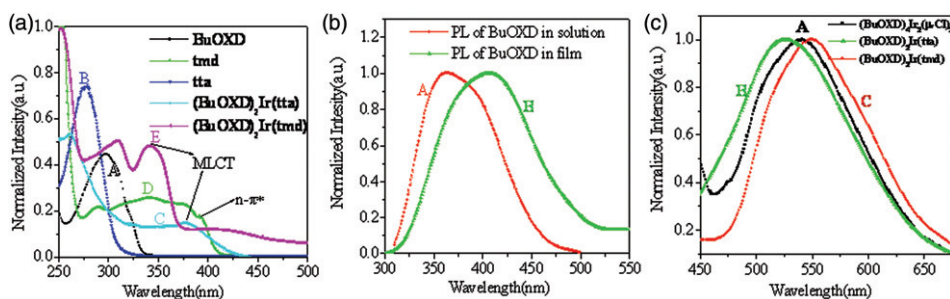
Figure 2. (a) Curve A: absorption spectrum of BuOXD; curve B: absorption spectrum of tta; curve C: absorption spectrum of $(BuOXD)_2Ir(tta)$; curve D: absorption spectrum of tmd; and curve E: absorption spectrum of $(BuOXD)_2Ir(tmd)$. (b) Curve A: PL spectra of ligand in solution; curve B: PL spectra of ligand in film. (c) Curve A: PL spectra of $(BuOXD)_4Ir_2(\mu-Cl)_2$; curve B: PL spectra of $(BuOXD)_2Ir(tta)$; and curve C: PL spectra of $(BuOXD)_2Ir(tmd)$ in CH_2Cl_2.

coupling [27]. By comparing curves B and C, the peak at 376 nm of curve C is due to the MLCT band of $(BuOXD)_2Ir(tta)$, which is of lowest energy and hence the emission in the $(BuOXD)_2Ir(tta)$ complex is Ir–CN centered. Also by comparing curves D and E the peak at 393 nm of curve D is due to a tmd centered $n–\pi^*$ electronic transition. The energy of these transitions is lower than the MLCT of $(BuOXD)_2Ir(tmd)$, and hence in $(BuOXD)_2Ir(tmd)$ the emission switched from Ir–CN center to ligand (tmd) center. Curves A and B of figure 2(b) show the PL spectra of BuOXD in CH_2Cl_2 and in film, respectively. In comparison to the PL spectrum in solution, the PL spectrum of the ligand in film shows bathochromic shift and broader emission. This may be attributed to stronger intermolecular interaction in the solid state, including hydrogen bonding and $\pi–\pi^*$ interactions between aromatic ligands of oxadiazole [28]. Figure 2(c) shows the PL emission spectra for dinuclear and mononuclear ($[C^\wedge N]_4Ir_2(\mu-Cl)_2]$, $[C^\wedge N]_2Ir(X)]$) complexes in CH_2Cl_2 at room temperature. All these complexes show strong luminescence from 500 to 600 nm. Emission bands from MLCT states are generally broad and featureless [29]. It is observed that changing the β-diketone in $[C^\wedge N]_2Ir(X)]$ typically has an effect on the maximum emission wavelength in the spectrum. Curve A in figure 2(c) is the PL spectrum of the $(BuOXD)_4Ir_2(\mu-Cl)_2$ complex showing λ_{max} at 540 nm. Curves B and C of figure 2(c) show the PL of $(BuOXD)_2Ir(tta)$ and $(BuOXD)_2Ir(tmd)$ with λ_{max} at 523 and 550 nm, respectively. This blue and red shift in λ_{max} of $(BuOXD)_2Ir(tta)$ and $(BuOXD)_2Ir(tmd)$, respectively, with respect to $(BuOXD)_4Ir_2(\mu-Cl)_2$ may be because of the difference in electronegativity of the groups attached to the β-diketone.

3.3. *Electroluminescent characterization*

1,3,4-Oxadiazoles generally emit light in the blue region of the electromagnetic spectrum. To study the EL of ligand and iridium complexes, electroluminescent devices were fabricated using the ligand or metal complexes as emissive layer materials. Eight percent metal complex doped CBP was used as emissive layer to avoid the concentration quenching of Ir–Ir metal. The device structure and thickness of the layers are as follows:

Device 1. ITO/α-NPD (300 Å)/BuOXD (350 Å)/BCP (60 Å)/Alq$_3$ (280 Å)/LiF (10 Å)/Al (1000 Å).
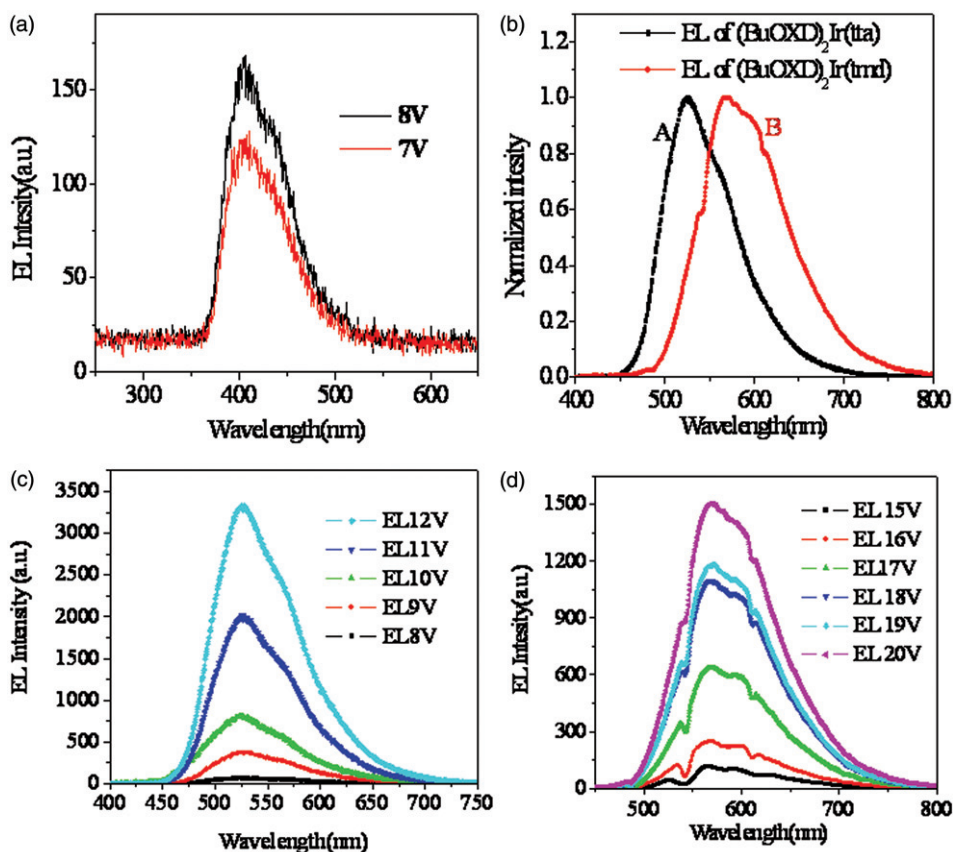
Figure 3. (a) EL spectra of BuOXD. (b) Curve A: normalized EL spectra of (BuOXD)$_2$Ir(tta) and curve B: normalized EL spectra of (BuOXD)$_2$Ir(tmd). (c) EL spectra of (BuOXD)$_2$Ir(tta) at various voltages. (d) EL spectra of (BuOXD)$_2$Ir(tmd) at various voltages.

Device 2. ITO/α-NPD (300 Å)/8% (BuOXD)$_2$Ir(tta) doped CBP (350 Å)/BCP (60 Å)/ Alq$_3$ (280 Å)/LiF (10 Å)/Al (1000 Å).
Device 3. ITO/α-NPD (300 Å)/8% (BuOXD)$_2$Ir(tmd) doped CBP (350 Å)/BCP (60 Å)/ Alq$_3$ (280 Å)/LiF (10 Å)/Al (1000 Å).

EL spectra of BuOXD, normalized EL spectra of (BuOXD)$_2$Ir(tta) and (BuOXD)$_2$Ir(tmd), EL spectra of (BuOXD)$_2$Ir(tta) at different voltage and EL spectra of (BuOXD)$_2$Ir(tmd) at different voltages are shown in figure 3(a)–(d), respectively. The BuOXD, (BuOXD)$_2$Ir(tta) and (BuOXD)$_2$Ir(tmd) show EL at 405, 526, and 570 nm, respectively. As shown in figure 3(b), device 2 having fluoro substituted dopant exhibits the expected blue shift as compared to that of device 3, which is consistent with the PL investigation. The EL emission spectra of the devices matched the PL emission spectra of the complexes in solution, which indicated that the EL emission is from the triplet excited states of the metal complexes. Figure 4 shows the schematic energy level diagram of the device structure used in this study. The LUMO of Alq$_3$ (3.0 eV) is almost matching with the LUMO of BCP (2.9 eV) and hence there is no barrier for electron transport. The barrier of 0.6 eV between BCP and the emissive layer leads to the
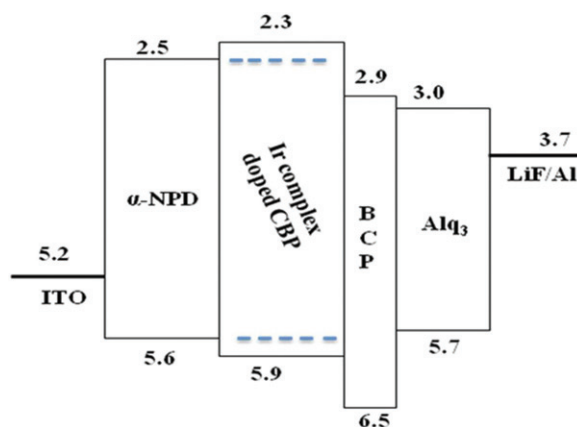
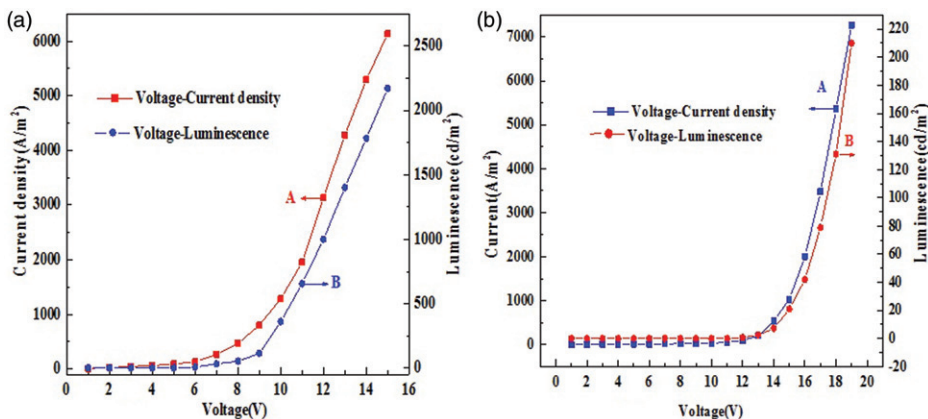Figure 4.   Schematic energy level diagram of the device used in this study.

Figure 5.   (a) Curve A, J–V and curve B, V–L characteristics of device using 8% $(BuOXD)_2Ir(tta)$ doped CBP as emissive material. (b) Curve A, J–V and curve B, V–L characteristics of device using 8% $(BuOXD)_2Ir(tmd)$ doped CBP as emissive material.

accumulation of electrons at the interface of BCP and emissive layer. Likewise, there is no barrier for holes coming from ITO to HTL and the emissive layer. But HOMO of BCP (6.5 eV) lies much below the HOMO of the emissive layer and therefore the emissive layer/BCP interface also acts as a barrier for holes coming from ITO resulting in limiting the recombination zone in the emissive layer. Furthermore, no emission from CBP was observed, indicating a complete energy transfer from the host exciton to the Ir-dopant. Meanwhile, there is no exciton decay in the Alq_3 layer due to the hole blocking action of the BCP layer. Hence Alq_3 and BCP do not contribute to the EL spectrum and act as electron transport and hole blocking layers, respectively.

Figure 5(a) shows the J–V–L characteristics of $(BuOXD)_2Ir(tta)$. Curve A shows the current–voltage and curve B shows the voltage–luminescence characteristics. From this figure it can be concluded that the device showed maximum luminescence of $2172 \, cdm^{-2}$ at 15 V. Figure 5(b) shows the J–V–L characteristics of $(BuOXD)_2Ir(tmd)$,
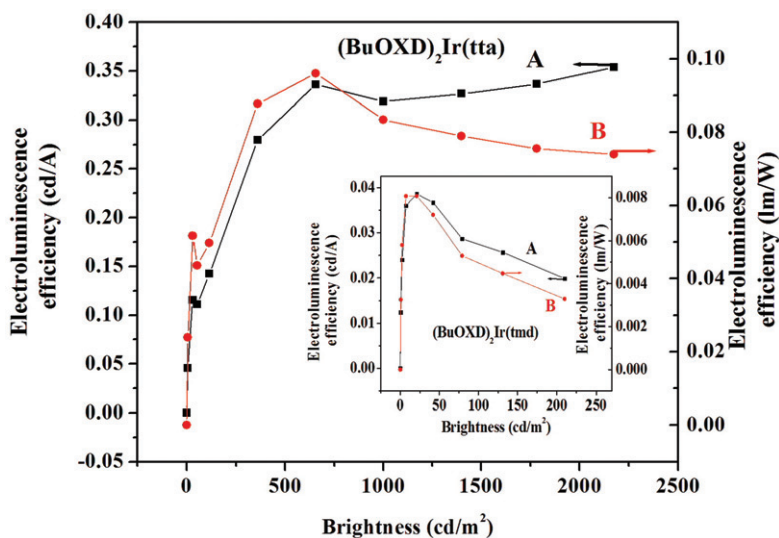
Figure 6. Curve A, CE–L and curve B, PE–L characteristics of device using 8% (BuOXD)$_2$Ir(tta) doped CBP as emissive material. Inset: Curve A, CE–L and curve B, PE–L characteristics of device using 8% (BuOXD)$_2$Ir(tmd) doped CBP as emissive material.

where curve A shows the current–voltage and curve B shows the voltage–luminescence characteristics. This figure shows that the device had a maximum luminescence of $210\,cd\,m^{-2}$ at 19 V. Figure 6 shows EL efficiency–brightness characteristics of the iridium complexes. Curves A and B show current efficiency and power efficiency with brightness of the device having (ButOXD)$_2$Ir(tta) as emissive material. The device shows maximum current efficiency $0.34\,cd\,A^{-1}$ at $657\,cd\,m^{-2}$. The inset of figure 6 shows the efficiencies of the device having (ButOXD)$_2$Ir(tmd) as emissive material. The efficiencies of the device having (ButOXD)$_2$Ir(tmd) are less than the device having (ButOXD)$_2$Ir(tta) as emissive material. This reduction in efficiencies can be attributed to switching of emission center from "$C^{\wedge}N_2$Ir" to X in (ButOXD)$_2$Ir(tmd).

4. Conclusion

Substitution on β-diketone with functional groups of different electronegativity alters the electronic properties of the complex, resulting in tuning the emission color. The present complexes are stable in air and can be deposited by thermal evaporation during device fabrication. Electroluminescent characteristics of these metal complexes show that these materials can be used as good emitting materials for OLED applications. This study provides a convenient way to tune the emission color by changing the secondary ligand.

Acknowledgments

References

[1] Y.-L. Tung, S.-W. Lee, Y. Chi, L.-S. Chen, C.-F. Shu, F.-I. Wu, A.J. Carty, P.-T. Chou, S.-M. Peng, G.-H. Lee. *Adv. Mater.*, **17**, 1059 (2005).

[2] P.-T. Chou, Y. Chi. *Eur. J. Inorg. Chem.*, 3319 (2006).

[3] S.-J. Yeh, M.-F. Wu, C.-T. Chen, Y.-H. Song, Y. Chi, M.-H. Ho, S.-F. Hsu, C.H. Chen. *Adv. Mater.*, **17**, 285 (2005).

[4] C.-L. Li, Y.-J. Su, Y.-T. Tao, P.-T. Chou, C.-H. Chien, C.-C. Cheng, R.-S. Liu. *Adv. Funct. Mater.*, **15**, 387 (2005).

[5] G. Zhou, W.-Y. Wong, B. Yao, Z. Xie, L. Wang. *Angew. Chem., Int. Ed.*, **46**, 1149 (2007).

[6] G. Zhang, H.-H. Chou, X. Jiang, P. Sun, C.-H. Cheng, Y. Ooyama, Y. Harima. *Org. Electron.*, **11**, 632 (2010).

[7] H.J. Bolink, E. Coronado, S.G. Santamaria, M. Sessolo, N. Evans, C. Klein, E. Baranoff, K. Kalyanasundaram, M. Graetzel, M.K. Nazeeruddin. *Chem. Commun.*, 3276 (2007).

[8] G. Ge, J. He, H. Guo, F. Wang, D. Zou. *J. Organomet. Chem.*, **694**, 3050 (2009).

[9] X. Zhang, J. Gao, C. Yang, L. Zhu, Z. Li, K. Zhang, J. Qin, H. You, M. Dongge. *J. Organomet. Chem.*, **691**, 4312 (2006).

[10] T.-H. Chuang, C.-H. Yang, P.-C. Kao. *Inorg. Chim. Acta.*, **362**, 5017 (2009).

[11] G. Zhang, F.-I. Wu, X. Jiang, P. Sun, C.-H. Cheng. *Synth. Met.*, **160**, 1906 (2010).

[12] K. Brunner, A.V. Dijken, H. Borner, J.J.A.M. Bastiaansen, N.M.M. Kiggen, B.M.W. Langeveld. *J. Am. Chem. Soc.*, **126**, 6035 (2004).

[13] W. Ma, P.K. Iyer, X. Gong, B. Liu, D. Moses, G.C. Bazan, A.J. Heeger. *Adv. Mater.*, **17**, 274 (2005).

[14] Z. Lü, Z. Deng, J. Zheng, D. Xu, Z. Chen, E. Zhou, Y. Wang. *Vacuum.*, **84**, 1287 (2010).

[15] Y. Wang, F. Teng, C. Ma, Z. Xu, Y. Hou, S. Yang, Y. Wang, X. Xu. *Displays.*, **25**, 237 (2004).

[16] S. Oyston, C. Wang, G. Hughes, A.S. Batsanov, I.F. Perepichk, M.R. Bryce, J.H. Ahn, C. Pearson, M.C. Petty. *J. Mater. Chem.*, **15**, 194 (2005).

[17] G. Hughes, M.R. Bryce. *J. Mater. Chem.*, **15**, 94 (2005).

[18] C. Wang, M. Kilitziraki, L.-O. Palsson, M.R. Bryce, A.P. Monkman, I.D.W. Samuel. *Adv. Funct. Mater.*, **11**, 47 (2001).

[19] J.C. Ostrowski, M.R. Robinson, A.J. Heeger, G.C. Bazan. *Chem. Commun.*, 784 (2002).

[20] L. Chen, H. You, C. Yang, D. Ma, J. Qin. *Chem. Commun.*, 1352 (2007).

[21] W. Ma, P.K. Iyer, X. Gong, B. Liu, D. Moses, G.C. Bazan, A.J. Heeger. *Adv. Mater.*, **17**, 274 (2005).

[22] S. Lamansky, P. Djurovich, D. Murphy, F.A. Razzaq, H.E. Lee, C. Adachi, P.E. Burrows, S.R. Forrest, M.E. Thompson. *J. Am. Chem. Soc.*, **123**, 4304 (2001).

[23] K. Dedeian, P.I. Djurovich, F.O. Garces, G. Carlson, R.J. Watts. *Inorg. Chem.*, **30**, 1685 (1991).

[24] Y. Fang, Y. Li, S. Wang, Y. Meng, J. Peng, B. Wang. *Synth. Met.*, **160**, 223 (2010).

[25] J.S. Park, M. Song, Y.S. Gal, J.W. Lee, S.H. Jin. *Synth. Met.*, **161**, 213 (2011).

[26] P. Zhang, B. Tang, W. Tian, B. Yang, M. Li. *Mater. Chem. Phys.*, **119**, 243 (2010).

[27] A.B. Tamayo, B.D. Alleyne, P.I. Djurovich, S. Lamansky, I. Tsyba, N.N. Ho, R. Bau, M.E. Thompson. *J. Am. Chem. Soc.*, **125**, 7377 (2003).

[28] L. Chen, C. Yang, M. Li, J. Qin, J. Gao, H. You, D. Ma. *Cryst. Growth Des.*, **7**, 39 (2007).

[29] H.-W. Hong, T.-M. Chen. *Mater. Chem. Phys.*, **101**, 170 (2007).